NANO LETTERS

pubs.acs.org/NanoLett

Letter

Structure of Polymer-Grafted Nanocellulose in the Colloidal Dispersion System

Shuji Fujisawa,* Yuichi Takasaki, and Tsuguyuki Saito

Cite This: *Nano Lett.* 2023, 23, 880−886

Read Online

ACCESS | Metrics & More | Article Recommendations | Supporting Information

ABSTRACT: Clarifying the primary structure of nanomaterials is invaluable to understand how the nanostructures lead to macroscopic material functions. Nanocellulose is attracting attention as a sustainable building block in materials science. The surface of nanocellulose is often chemically modified by polymer grafting to tune the material properties, such as the viscoelastic properties in rheology modifiers and the reinforcement effect in composites. However, the structure, such as molecular conformation of the grafted polymer and the twist of the core nanocellulose, is not well understood. Here, we investigated the structure of polymer-grafted nanocellulose in the colloidal dispersion system by combining small-angle X-ray scattering measurement and all-atom molecular dynamics simulation. We demonstrated formation of the polymer brush layer on the nanocellulose surface in solvents, which explains the excellent colloidal stability. We also found that twisting of the nanocellulose in the core is suppressed by the existence of the polymer brush layer.

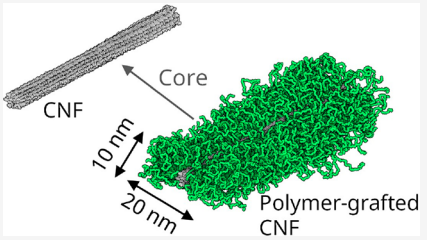

KEYWORDS: *Molecular dynamics simulation, Nanocellulose, Polymer grafting, Small-angle X-ray scattering*

Cellulose nanofiber (CNF), a naturally occurring crystalline fibril, has been attracting attention as a sustainable building block in advanced materials science.[1−4] CNFs are obtained from plants by disassembling the natural hierarchical structures of the cell walls. In the case of trees, the resultant CNF exhibits a width of only ∼3 nm and a length of up to several micrometers, possessing a crystalline nanofibrillar structure composed of only a few tens of cellulose molecular chains.[5,6] Owing to the crystal structure, the axial modulus and strength of an individual CNF are as high as 110−140 and 2−3 GPa,[5,7] respectively. The excellent mechanical properties and unique nanosized morphology of CNF offer a number of potential applications including nanofillers in composite materials, high-performance packaging films, and rheology modifiers.[1,2,8−11]

Controlling the colloidal stability of CNF is needed to efficiently develop its functionalities, such as the viscoelastic properties in rheology modifiers and the reinforcement effect in composites. Chemical modification of the CNF surface not only can change the surface properties but can also increase the repulsive forces between CNFs. Typically, anionic or cationic functional groups are introduced on the surface of CNFs to achieve colloidal stability in water or polar organic solvents.[12] However, these CNFs rapidly aggregate in low-polarity organic solvents, in which electric double layer repulsion between the CNFs is significantly weakened.

The colloidal stability in low-polarity organic solvents is dramatically enhanced by grafting a long polymer on an individual CNF unit.[1,12,13] The grafted CNFs are individually dispersed in the solvents of various polarities, which is mainly driven by steric repulsion, and form macroscopically stable dispersions. The dispersions not only allow homogeneous mixing with other materials, such as polymers but also realize idealized interfacial stress transfer in the final composites.[14] Because the grafted polymer chains induce colloidal stability in the dispersion, clarifying the molecular conformation of the grafted chains is the key to understanding how the nanoarchitectures lead to macroscopic functions. However, how the grafted polymers are structured on the surface of an individual CNF is not understood owing to the complex molecular arrangement of the polymers in the dispersed system.

Here, we report the structure of polymer-grafted CNF in the colloidal dispersion system. Combining small-angle X-ray scattering (SAXS) measurement and all-atom molecular dynamics (MD) simulation, we visualized the structure, not only the conformation of the CNF and grafted polymer chain but also the chemical bonding between them. We found that a polymer brush layer formed on the CNF surface. The brush layer induced the colloidal stability in low-polarity solvents and also suppressed twisting of the core CNF. These results will be helpful not only for understanding CNF structures but also for bottom-up design of advanced CNF-based materials that satisfy sustainability requirements.

Received: October 21, 2022
Revised: December 12, 2022
Published: December 15, 2022

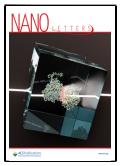

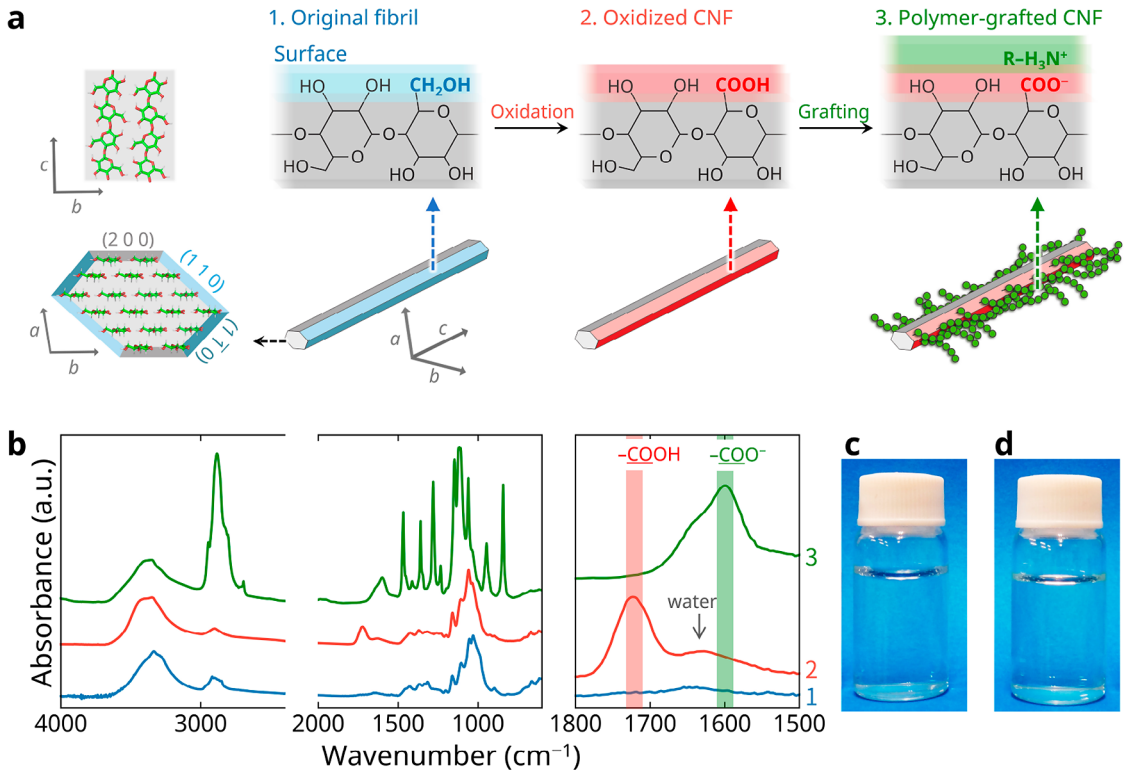

Figure 1. Polymer grafting onto the CNF surface. (a) Schematic of preparation of polymer-grafted CNF, illustrated with a CNF model containing 18 cellulose chains.[21,22] The primary hydroxy groups exposed on the (1 1 0) and (1 $\bar{1}$ 0) surfaces (light and dark blue, respectively) were selectively converted to carboxy groups (light and dark red, respectively) by TEMPO-mediated oxidation. Amine-terminated PEG (R = $-(CH_2)_3-(OC_2H_4)_{48}-OCH_3$) chains were end-grafted onto the carboxy groups through ionic bonds. (b) FT-IR spectra of the original cellulose (softwood bleached kraft pulp, blue), oxidized CNF (red), and polymer-grafted CNF (green). Photograph of a 1% w/w polymer-grafted CNF dispersion in (c) water and (d) tetrahydrofuran.

The fabrication steps of the polymer-grafted CNF are shown in Figure 1a. In nature, cellulose molecular chains assemble into crystalline nanofibers, which are called cellulose microfibrils. The microfibrils from wood predominantly consist of cellulose I_β,[15,16] which has a monoclinic unit cell and C6 primary hydroxy groups exposed on the (1 1 0) and (1 $\bar{1}$ 0) surfaces. The primary hydroxy groups on the surface were selectively oxidized to carboxy groups through 2,2,6,6-tetramethylpiperidin-1-oxyl (TEMPO)-mediated oxidation.[17] The introduced carboxy groups act as anchoring sites for immobilizing amine-terminated polyethylene glycol (PEG) chains. The PEG chains were selectively introduced onto the surface carboxy groups, which was confirmed by Fourier transform infrared (FT-IR) spectroscopy (Figure 1b); the peak due to the PEG chains appeared after the grafting, and the carbonyl stretching band of COOH groups on the CNF surfaces (1720 cm^{-1})[18] was entirely shifted to that of COO^- groups (1600 cm^{-1}), which demonstrates the formation of ionic bond.[19] The surface PEG chains enable control over CNF aggregation, yielding stable dispersions in solvents with various polarities, such as water (Figure 1c), tetrahydrofuran (THF, Figure 1d), chloroform, and toluene.[20]

To gain structural insights into the polymer-grafted CNF in the dispersion system, we performed all-atom MD simulation. The MD simulation is a powerful tool for investigating dynamics and conformation of molecules in cellulose crystallites. A number of studies have been conducted to understand the structure of CNF with various kinds of crystal sizes.[23−28] In this study, the CHARMM carbohydrate force field, which is one of the most widely used force fields for cellulose,[27,29−32] was used to study the structure of the polymer grafted CNF. First, we placed the initial structure (Figure 2a) in a periodic box with dimensions of 22 nm × 28 nm × 60 nm, and the box was solvated with THF molecules. Then, an MD production run for 15 ns was performed and the final structure was obtained (Figure 2b and Figure S1 in Supporting Information). The simulation results showed that the CNF core finally twisted (Figure 2a,b).[33] In the early steps of the simulation, the CNF started to twist in a right-handed manner. The twist angle along the fiber axis per cellobiose unit (θ_{twist}) plateaued at ∼1° after 10 ns of the simulation (Figure 2c and Figure S2 in the Supporting Information). The MD simulation suggested that the PEG chains were stretched and formed a polymer brush layer on the CNF surface. This is because the average distance between two adjacent carboxy groups on the surface (∼0.8 nm)[17,20] is smaller than the radius of gyration (R_g) of free or sparsely end-grafted PEG chains in THF (1.7 nm; see Figure S3), which is determined by MD simulation. Therefore, the PEG chains grafted on the CNF were forced to stretch away from the surface. The thickness of the PEG brush layer was ∼10 nm, which is consistent with the value of ∼11 nm calculated by the theory of end-grafted polymer brushes.[34] In general, the repulsive force between grafted polymer brush layers depends on the thickness and density of the polymer layer. When short alkyl chains are grafted onto the CNF, the grafted-CNFs cannot be dispersed in THF, chloroform, and toluene, even though the grafting density is the same as that in this study.[19] Therefore, the PEG

https://doi.org/10.1021/acs.nanolett.2c04138
Nano Lett. 2023, 23, 880−886

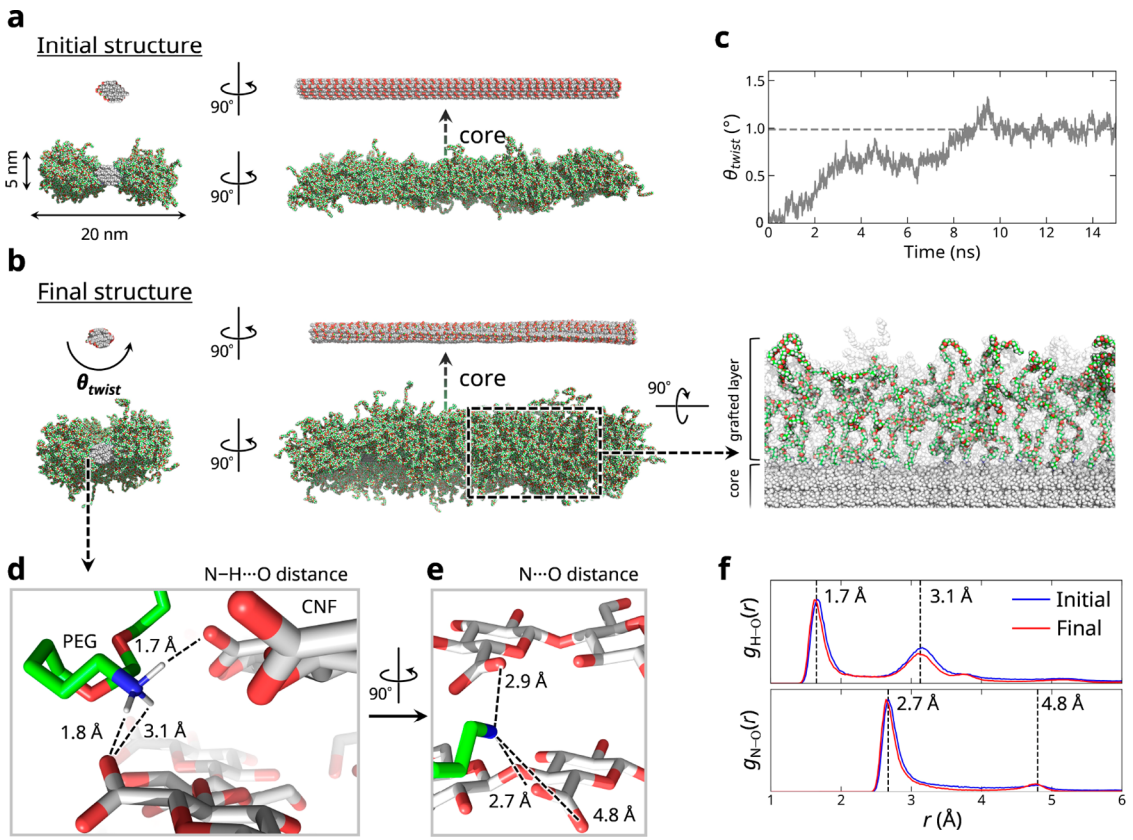

Figure 2. Structure of polymer-grafted CNF from the all-atom MD simulation. (a) Initial structure. The structure was obtained by pre-equilibrating the polymer-grafted CNF in THF for 10 ns while applying position restraint only to the CNF core using a force constant of 1000 kJ mol^{-1} nm^{-2}. (b) Simulated structure obtained by equilibrating the initial structure in THF for 15 ns without any position restraint so that the core CNF started to twist. (c) Change of the calculated value of θ_{twist}/cellobiose unit with time. (d, e) Magnified interface showing the molecular details of the interaction between amine-terminated PEG and the CNF. Oxygen, nitrogen, the hydrogen atoms of the ammonium group, the carbon atoms of the CNF, and the carbon atoms of PEG are colored red, blue, white, gray, and green, respectively. (f) Radial distribution functions between the ammonium hydrogen and carboxylate oxygen atoms $g_{H-O}(r)$, and the ammonium nitrogen and carboxylate oxygen atoms $g_{N-O}(r)$ before and after the simulation. The functions were extracted from the final 1 ns of the trajectories.

layer in this work seemed to be sufficiently thick to prevent aggregation of the CNFs even in THF. This was corroborated by the experimentally observed high colloidal stability of the grafted CNF dispersion system without any appreciable aggregation for over a year (Figure S4). The long-term colloidal stability has been confirmed also in chloroform and toluene.[20]

The representative structures at the polymer−CNF interface are shown in Figure 2d,e. The ammonium and carboxylate groups formed ion pairs with electrostatic interactions ($N^+\cdots O^-$), together with hydrogen bonds ($N^+-H\cdots O^-$). The radial distribution functions extracted from the simulation results showed a distance of 2.7 Å between the carboxylate and ammonium groups ($N^+\cdots O^-$) and a hydrogen-bond length of 1.7 Å ($N^+-H\cdots O^-$) (Figure 2f), which are consistent with Figure 2d,e. This combined interaction is a so-called salt bridge,[35,36] which is well-known in protein and supramolecular chemistry. It should be noted that almost all of the ammonium groups formed another salt bridge with a carboxylate group neighboring the cellulose molecular sheets. Formation of an ion pair is mainly driven by entropic contributions through desolvation of the ions.[37] Therefore, it is likely that the system thermodynamically favored more interactions with the closely neighboring (~0.7 nm) carboxylate groups. The radial distribution functions $g_{H\cdots O}(r)$ and $g_{N\cdots O}(r)$ showed second largest peaks at 3.1 and 4.8 Å, respectively, which correspond to the other combination of the atoms between the ammonium and carboxylate groups, as described in Figure 2d,e. Interestingly, the radial distribution functions of the initial and final structures exhibited almost the same peak shapes and positions (Figure 2f). Furthermore, the R_g value of the grafted PEG remained unchanged from that of the initial structure (Figure 3). Thus, during the simulation, twisting of the core CNF exclusively occurred, maintaining the PEG/CNF interaction and PEG brush conformation.

To compare the predicted structure with experimental data, we performed SAXS analysis. The experimental SAXS curves of polymer-grafted CNF dispersed in THF are shown in Figure 4. Two types of dispersions with CNF concentrations of 0.5% and 1.0% w/v were prepared, and the shapes of the scattering curves were the same (Figure 4a). This demonstrates that the structure factor, which describes interference scattering between the particles (polymer-grafted CNFs in this case),[38] can be ignored and that the cross-sectional size and shape of the polymer-grafted CNFs remained unchanged in this concentration range.

To rationalize the experimentally obtained SAXS curves, we calculated the theoretical SAXS pattern from all of the atoms in the simulated structure. Notably, the calculated SAXS pattern agreed well with the experimentally obtained patterns (Figure

https://doi.org/10.1021/acs.nanolett.2c04138
Nano Lett. 2023, 23, 880−886

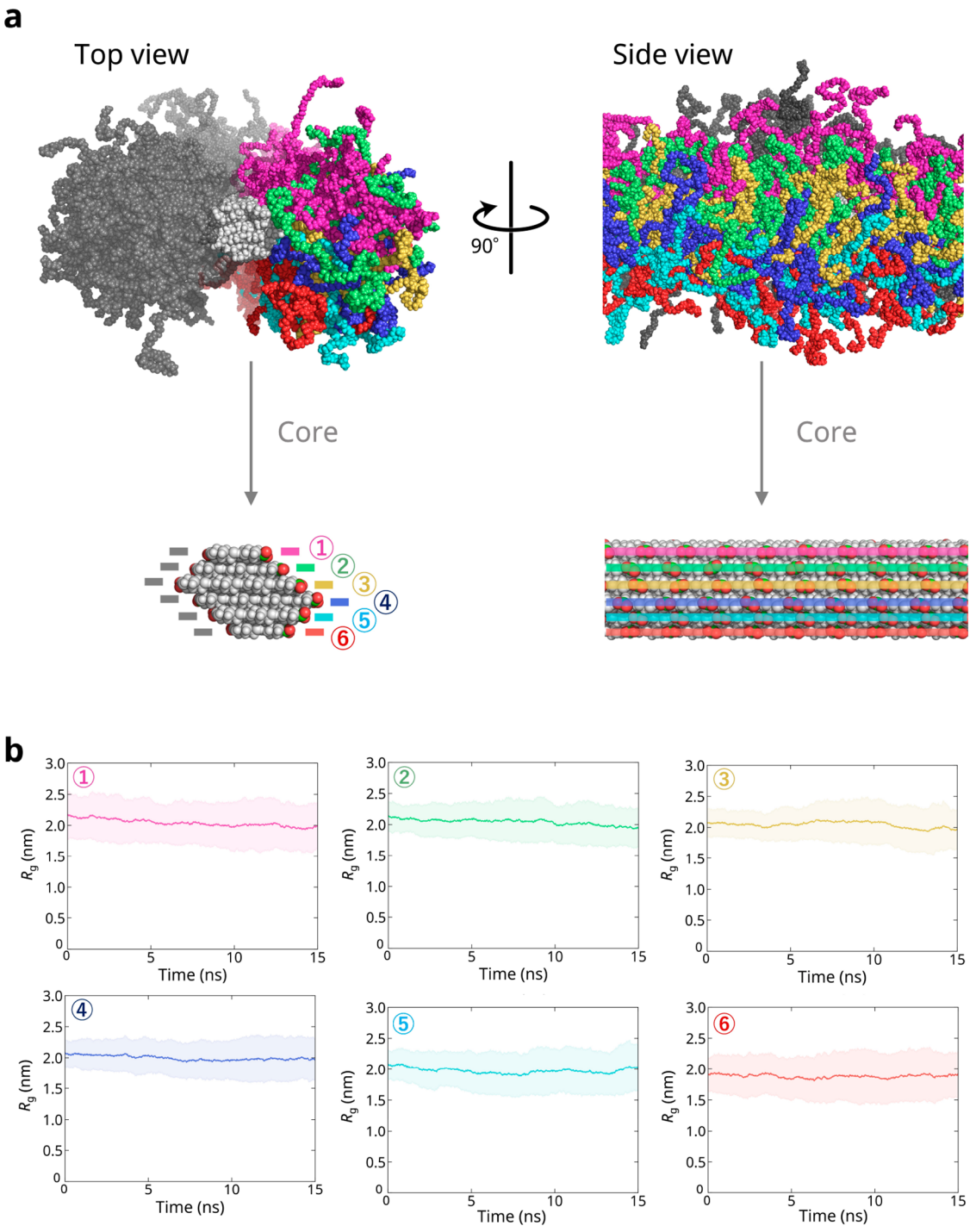

Figure 3. Radius of gyration (R_g) of grafted PEG in the simulated structure. (a) PEG molecules along one side of the CNF categorized into six groups, with the PEG molecules end-grafted to the same oxidized cellulose chain grouped into the same group. (b) Time evolution of R_g for the surface PEG chain in the production run for 15 ns. The data are expressed as the mean ± the standard deviation, obtained from 40 PEG chains grafted on each oxidized cellulose chain.

4a). The slopes showed excellent agreement in wide q ranges (Figure 4b,c). The calculated scattering pattern changed with the increase of the twist angle of the CNF core (Figure S5), and the pattern of the final structure was in the best agreement with the experimentally obtained patterns. This emphasized that the twist angle of the CNF core was well reproduced by the simulation. In the range of $2 < q < 7$ nm^{-1}, the slope of the double logarithmic plot provides information about the surface smoothness at the molecular scale, which can be described by a surface fractal dimension.[39] The slope from the MD simulation was in good agreement with the experimental results, demonstrating that the surface smoothness of the brush layer was also well modeled by the simulation.

We also fitted the experimentally obtained SAXS patterns using simple cylinder models with uniform electron density (Figure 5). However, the fitting was not satisfactory, probably because these models were insufficient to recreate the scattering curves in the Porod region originating from the

https://doi.org/10.1021/acs.nanolett.2c04138
Nano Lett. 2023, 23, 880−886

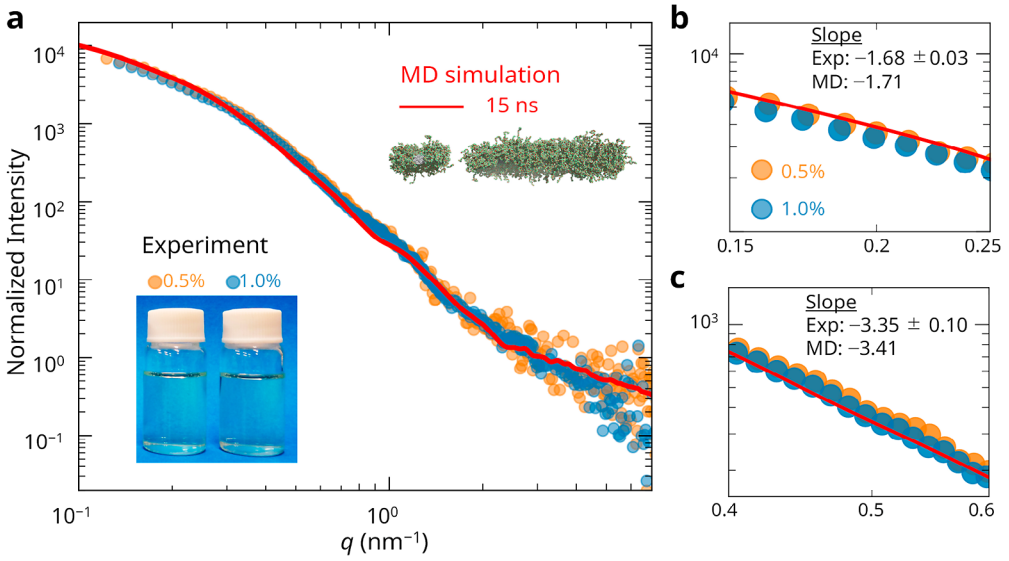

Figure 4. SAXS measurement of the polymer-grafted CNF in the dispersion system. (a) Experimental SAXS patterns with concentration-normalized intensity, along with the calculated SAXS pattern from the final structure of the MD simulation (red line). (b, c) Magnified SAXS patterns in the q ranges of 0.15−0.25 and 0.4−0.6 nm^{-1}. The MD structure was able to accurately reproduce the experimentally obtained SAXS curves of the polymer-grafted CNF.

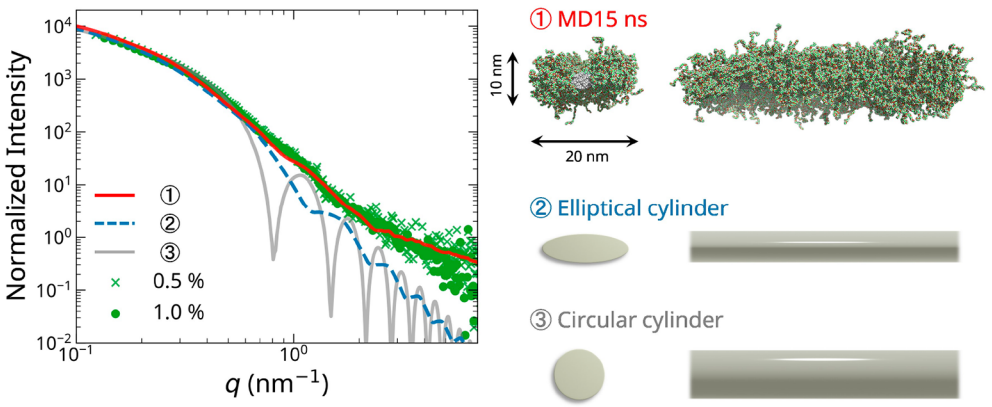

Figure 5. Fitting results using simple cylinder models. The experimental data of the 1.0% w/w polymer-grafted CNF dispersion were fitted to elliptical and circular cylinder models. The best fits for the lower q region profiles (an elliptical cylinder with a radius of 3.0 nm and an axis ratio of 3 and a circular cylinder with a radius of 4.7 nm) are shown.

complex surface molecular structure. The hybrid method combining SAXS measurement and MD simulation is much more suitable for clarifying the molecular details of surface grafted CNFs.

The scattering patterns in the q range of 0.15−1.5 nm^{-1}, which contains information about the cross-sectional shape of the polymer-grafted CNF, showed no dependence on the concentration (Figure 4). This shows that the concentration range of 0.5−1.0% w/v is valid for form-factor analysis. The validity is also supported by neutron scattering analysis of surfactant-coated cellulose whiskers,[40] in which the concentration of cellulose was varied from 0.2% to 1.5% w/w.

The simulated structure showed right-handed twisting along the axis (Figure 2), and θ_{twist} of the final structure was 1.0° per cellobiose unit, which suggests twisting of the CNF in the dispersion system. Significant effort has been devoted to analyze twisting of CNFs, not only by experimental microscopic observation in dried[33,41−43] or cryogenic[44,45] systems but also by MD simulation in vacuum or aqueous systems.[25−27] Interestingly, our θ_{twist} value was smaller than those previously obtained by MD simulations. The θ_{twist} value significantly depends on the model dimensions, and θ_{twist} increases with decreasing cross section.[25,26] In the case of the CNF model with 18 chains, θ_{twist} has been reported to be 4.6° per cellobiose unit,[27] which is larger than the value of the polymer-grafted CNF in this study. When a pristine CNF, which was not grafted with PEG chains but contained sodium ions as counter cations, was used for simulation of twisting, the θ_{twist} value of the CNF was 4.7°, which is similar to the previously reported values[25−27] (see Figure S6). Therefore, twisting of the CNF core was suppressed by the existence of the bulky polymer layer, probably because of steric repulsion between the brush layers on both sides of the CNF core brought into closer contact by twisting of the CNF core.

In conclusion, we have clarified the structure of polymer-grafted CNF in the colloidal dispersion system through a combination of SAXS measurement and MD simulation. The experimental results were well rationalized by the simulation, and not only the conformation of PEG and the CNF but also the interaction at the PEG−CNF interface were investigated.

https://doi.org/10.1021/acs.nanolett.2c04138
Nano Lett. 2023, 23, 880−886

The amine-terminated PEG chains were anchored on the surface of the CNF through a salt-bridge structure with carboxylate groups. The densely grafted structure allowed formation of a polymer brush layer on the CNF, which explains the good colloidal stability in solvents. It was found that the existence of the brush layer affects the conformation of the CNF, and twisting of the CNF core is suppressed in the grafted system. Our approach through combined computational and experimental analysis is applicable to other systems such as the colloidal dispersions in toluene and chloroform, and the versatility of this method will allow us to understand the CNF structures in various media. Moreover, the knowledge of the structures and dynamics may give insights into the assembly behavior of the CNFs during preparation of the materials such as films, gels, and composites, which will lead to development of advanced mechanical, thermal, and optical properties in the materials. Therefore, these results will be helpful not only for understanding the mechanism of colloidal stabilization but also for better design of CNF-based materials from dispersions.

■ ASSOCIATED CONTENT

Supporting Information

The Supporting Information is available free of charge at https://pubs.acs.org/doi/10.1021/acs.nanolett.2c04138.

Description of the materials, sample preparation, and methods, procedure for the MD simulation, definition of the twist angle of the CNF, R_g of the PEG-NH_3 molecule, photograph of polymer-grafted CNF stored for over a year, calculated SAXS profile, details of the SAXS fitting, and twisting of the pristine CNF (PDF)

■ AUTHOR INFORMATION

Corresponding Author

Shuji Fujisawa − *Department of Biomaterial Sciences, Graduate School of Agricultural and Life Sciences, The University of Tokyo, Tokyo 113-8657, Japan;* orcid.org/0000-0002-5221-6781; Email: afujisawa@g.ecc.u-tokyo.ac.jp

Authors

Yuichi Takasaki − *Business Unit Characterization, Anton-Paar Japan, Tokyo 131-0034, Japan*

Tsuguyuki Saito − *Department of Biomaterial Sciences, Graduate School of Agricultural and Life Sciences, The University of Tokyo, Tokyo 113-8657, Japan;* orcid.org/0000-0003-1073-6663

Complete contact information is available at: https://pubs.acs.org/10.1021/acs.nanolett.2c04138

Author Contributions

S.F. conceived the project. S.F. prepared the samples, performed data analysis of the SAXS measurement, and performed the MD simulations. Y.T. performed the SAXS measurement and data analysis. All authors discussed the data and wrote the manuscript.

Notes

The authors declare no competing financial interest.

■ ACKNOWLEDGMENTS

This study was supported by Grants-in-Aid for Scientific Research (Grant JP20K15567 to S.F. and Grant JP21H04733 to T.S.) from the Japan Society for the Promotion of Science (JSPS), the Japan Science and Technology Agency (JST)-Mirai R&D Program (Grant JPMJMI17ED to T.S. and S.F.), and JST CREST (Grant JPMJCR22L3 to T.S. and S.F.).

■ REFERENCES

(1) Moon, R. J.; Martini, A.; Nairn, J.; Simonsen, J.; Youngblood, J. Cellulose nanomaterials review: Structure, properties and nanocomposites. *Chem. Soc. Rev.* **2011**, *40*, 3941−3994.

(2) Klemm, D.; Kramer, F.; Moritz, S.; Lindström, T.; Ankerfors, M.; Gray, D.; Dorris, A. Nanocelluloses: A new family of nature-based materials. *Angew. Chemie - Int. Ed.* **2011**, *50*, 5438−5466.

(3) Heise, K.; Kontturi, E.; Allahverdiyeva, Y.; Tammelin, T.; Linder, M. B.; Nonappa; Ikkala, O. Nanocellulose: Recent Fundamental Advances and Emerging Biological and Biomimicking Applications. *Adv. Mater.* **2021**, *33*, 2004349.

(4) Thomas, B.; Raj, M. C.; B, A. K.; H, R. M.; Joy, J.; Moores, A.; Drisko, G. L.; Sanchez, C. Nanocellulose, a Versatile Green Platform: From Biosources to Materials and Their Applications. *Chem. Rev.* **2018**, *118*, 11575−11625.

(5) Nishiyama, Y. Structure and properties of the cellulose microfibril. *J. Wood Sci.* **2009**, *55*, 241−249.

(6) Cosgrove, D. J. Building an extensible cell wall. *Plant Physiol.* **2022**, *189*, 1246−1277.

(7) Saito, T.; Kuramae, R.; Wohlert, J.; Berglund, L. A.; Isogai, A. An ultrastrong nanofibrillar biomaterial: The strength of single cellulose nanofibrils revealed via sonication-induced fragmentation. *Biomacromolecules* **2013**, *14*, 248−253.

(8) Eichhorn, S. J. Cellulose nanowhiskers: Promising materials for advanced applications. *Soft Matter* **2011**, *7*, 303−315.

(9) Azizi Samir, M. A. S.; Alloin, F.; Dufresne, A. Review of recent research into cellulosic whiskers, their properties and their application in nanocomposite field. *Biomacromolecules* **2005**, *6*, 612−626.

(10) Ahankari, S. S.; Subhedar, A. R.; Bhadauria, S. S.; Dufresne, A. Nanocellulose in food packaging: A review. *Carbohydr. Polym.* **2021**, *255*, 117479.

(11) Xu, T.; Du, H.; Liu, H.; Liu, W.; Zhang, X.; Si, C.; Liu, P.; Zhang, K. Advanced Nanocellulose-Based Composites for Flexible Functional Energy Storage Devices. *Adv. Mater.* **2021**, *33*, 2101368.

(12) Habibi, Y. Key advances in the chemical modification of nanocelluloses. *Chem. Soc. Rev.* **2014**, *43*, 1519−1542.

(13) Yang, X.; Biswas, S. K.; Han, J.; Tanpichai, S.; Li, M. C.; Chen, C.; Zhu, S.; Das, A. K.; Yano, H. Surface and Interface Engineering for Nanocellulosic Advanced Materials. *Adv. Mater.* **2021**, *33*, 2002264.

(14) Biswas, S. K.; Tanpichai, S.; Witayakran, S.; Yang, X.; Shams, M. I.; Yano, H. Thermally superstable cellulosic-nanorod-reinforced transparent substrates featuring microscale surface patterns. *ACS Nano* **2019**, *13*, 2015−2023.

(15) Sugiyama, J.; Vuong, R.; Chanzy, H. Electron Diffraction Study on the Two Crystalline Phases Occurring in Native Cellulose from an Algal Cell Wall. *Macromolecules* **1991**, *24*, 4168−4175.

(16) Wada, M.; Sugiyama, J.; Okano, T. The monoclinc phase is dominant in wood cellulose. *Mokuzai Gakkaishi* **1994**, *40*, 50−56.

(17) Okita, Y.; Saito, T.; Isogai, A. Entire surface oxidation of various cellulose microfibrils by TEMPO-mediated oxidation. *Biomacromolecules* **2010**, *11*, 1696−1700.

(18) Fujisawa, S.; Okita, Y.; Fukuzumi, H.; Saito, T.; Isogai, A. Preparation and characterization of TEMPO-oxidized cellulose nanofibril films with free carboxyl groups. *Carbohydr. Polym.* **2011**, *84*, 579−583.

(19) Fujisawa, S.; Saito, T.; Isogai, A. Nano-dispersion of TEMPO-oxidized cellulose/aliphatic amine salts in isopropyl alcohol. *Cellulose* **2012**, *19*, 459−466.

(20) Fujisawa, S.; Saito, T.; Kimura, S.; Iwata, T.; Isogai, A. Surface engineering of ultrafine cellulose nanofibrils toward polymer nanocomposite materials. *Biomacromolecules* **2013**, *14*, 1541−1546.

(21) Daicho, K.; Saito, T.; Fujisawa, S.; Isogai, A. The crystallinity of nanocellulose: dispersion-induced disordering of the grain boundary

in biologically structured cellulose. *ACS Appl. Nano Mater.* **2018**, *1*, 5774−5785.
(22) Song, B.; Zhao, S.; Shen, W.; Collings, C.; Ding, S. Y. Direct Measurement of Plant Cellulose Microfibril and Bundles in Native Cell Walls. *Front. Plant Sci.* **2020**, *11*, 479.
(23) Oehme, D. P.; Yang, H.; Kubicki, J. D. An evaluation of the structures of cellulose generated by the CHARMM force field: comparisons to in planta cellulose. *Cellulose* **2018**, *25*, 3755−3777.
(24) Oehme, D. P.; Downton, M. T.; Doblin, M. S.; Wagner, J.; Gidley, M. J.; Bacic, A. Unique aspects of the structure and dynamics of elementary Iβ cellulose microfibrils revealed by computational simulations. *Plant Physiol.* **2015**, *168*, 3−17.
(25) Bu, L.; Himmel, M. E.; Crowley, M. F. The molecular origins of twist in cellulose I-beta. *Carbohydr. Polym.* **2015**, *125*, 146−152.
(26) Hadden, J. A.; French, A. D.; Woods, R. J. Unraveling cellulose microfibrils: A twisted tale. *Biopolymers* **2013**, *99*, 746−756.
(27) Kannam, S. K.; Oehme, D. P.; Doblin, M. S.; Gidley, M. J.; Bacic, A.; Downton, M. T. Hydrogen bonds and twist in cellulose microfibrils. *Carbohydr. Polym.* **2017**, *175*, 433−439.
(28) Paavilainen, S.; Róg, T.; Vattulainen, I. Analysis of twisting of cellulose nanofibrils in atomistic molecular dynamics simulations. *J. Phys. Chem. B* **2011**, *115*, 3747−3755.
(29) Gross, A. S.; Chu, J. W. On the molecular origins of biomass recalcitrance: The interaction network and solvation structures of cellulose microfibrils. *J. Phys. Chem. B* **2010**, *114*, 13333−13341.
(30) Langan, P.; Petridis, L.; O'Neill, H. M.; Pingali, S. V.; Foston, M.; Nishiyama, Y.; Schulz, R.; Lindner, B.; Hanson, B. L.; Harton, S.; Heller, W. T.; Urban, V.; Evans, B. R.; Gnanakaran, S.; Ragauskas, A. J.; Smith, J. C.; Davison, B. H. Common processes drive the thermochemical pretreatment of lignocellulosic biomass. *Green Chem.* **2014**, *16*, 63−68.
(31) Silveira, R. L.; Stoyanov, S. R.; Kovalenko, A.; Skaf, M. S. Cellulose Aggregation under Hydrothermal Pretreatment Conditions. *Biomacromolecules* **2016**, *17*, 2582−2590.
(32) Lee, C. M.; Kubicki, J. D.; Fan, B.; Zhong, L.; Jarvis, M. C.; Kim, S. H. Hydrogen-Bonding Network and OH Stretch Vibration of Cellulose: Comparison of Computational Modeling with Polarized IR and SFG. *Spectra. J. Phys. Chem. B* **2015**, *119*, 15138−15149.
(33) Hanley, S. J.; Revol, J. F.; Godbout, L.; Gray, D. G. Atomic force microscopy and transmission electron microscopy of cellulose from Micrasterias denticulata; evidence for a chiral helical microfibril twist. *Cellulose* **1997**, *4*, 209−220.
(34) de Gennes, P. G. Conformations of Polymers Attached to an Interface. *Macromolecules* **1980**, *13*, 1069−1075.
(35) Kumar, S.; Nussinov, R. Close Range Electrostatic Interactions in Proteins. *ChemBioChem* **2002**, *3*, 604−617.
(36) Donald, J. E.; Kulp, D. W.; DeGrado, W. F. Salt bridges: Geometrically specific, designable interactions. *Proteins Struct. Funct. Bioinforma.* **2011**, *79*, 898−915.
(37) Marcus, Y.; Hefter, G. Ion pairing. *Chem. Rev.* **2006**, *106*, 4585−4621.
(38) Glatter, O. The interpretation of real-space information from small-angle scattering experiments. *J. Appl. Crystallogr.* **1979**, *12*, 166−175.
(39) Martin, J. E.; Hurd, A. J. Scattering from fractals. *J. Appl. Crystallogr.* **1987**, *20*, 61−78.
(40) Bonini, C.; Heux, L.; Cavaillé, J. Y.; Lindner, P.; Dewhurst, C.; Terech, P. Rodlike cellulose whiskers coated with surfactant: A small-angle neutron scattering characterization. *Langmuir* **2002**, *18*, 3311−3314.
(41) Usov, I.; Nyström, G.; Adamcik, J.; Handschin, S.; Schütz, C.; Fall, A.; Bergström, L.; Mezzenga, R. Understanding nanocellulose chirality and structure-properties relationship at the single fibril level. *Nat. Commun.* **2015**, *6*, 7564.
(42) Arcari, M.; Zuccarella, E.; Axelrod, R.; Adamcik, J.; Sánchez-Ferrer, A.; Mezzenga, R.; Nyström, G. Nanostructural Properties and Twist Periodicity of Cellulose Nanofibrils with Variable Charge Density. *Biomacromolecules* **2019**, *20*, 1288−1296.
(43) Willhammar, T.; Daicho, K.; Johnstone, D. N.; Kobayashi, K.; Liu, Y.; Midgley, P. A.; Bergström, L.; Saito, T. Local Crystallinity in Twisted Cellulose Nanofibers. *ACS Nano* **2021**, *15*, 2730−2737.
(44) Elazzouzi-Hafraoui, S.; Nishiyama, Y.; Putaux, J. L.; Heux, L.; Dubreuil, F.; Rochas, C. The shape and size distribution of crystalline nanoparticles prepared by acid hydrolysis of native cellulose. *Biomacromolecules* **2008**, *9*, 57−65.
(45) Ogawa, Y. Electron microdiffraction reveals the nanoscale twist geometry of cellulose nanocrystals. *Nanoscale* **2019**, *11*, 21767−21774.

https://doi.org/10.1021/acs.nanolett.2c04138
Nano Lett. 2023, 23, 880−886